This article has been accepted for publication in a future issue of this journal, but has not been fully edited. Content may change prior to final publication. Citation information: DOI 10.1109/TAP.2019.2902623, IEEE Transactions on Antennas and Propagation

Design of a Portable Verification Artifact for Millimeter-Wave-Frequency Channel Sounders[1]

Jos N.H. Dortmans, *Student Member, IEEE*, Jeanne T. Quimby, *Member, IEEE*, Kate A. Remley, *Fellow, IEEE,* and Dylan F. Williams, *Fellow, IEEE*, Jelena Senic, Ruoyu Sun, *Senior Member, IEEE*, and Peter B. Papazian, *Senior Member IEEE*

***Abstract*— We developed a portable and traceable artifact for the conducted verification of millimeter-wave-frequency channel sounders under static conditions. The artifact is designed to create several multipath profiles with a direct path and up to two multipath components to be used during the verification of a channel sounder. The verification artifact shows that the channel sounder we tested measures extra multipath components possibly due to internal reflections in the channel sounder. While these differences are not likely to significantly change most channel metrics, they do indicate nonidealities in the channel sounder that might need to be addressed, depending on the application.**

***Index Terms*—5G technology; channel sounder; millimeter-wave wireless communication; propagation channel; wireless system.**

I. Introduction

THE use of wireless communications has grown enormously in recent years. In 2015, the global mobile data traffic grew by 74% [1], and this trend is expected to continue in the future. To be able to keep up with the use of wireless communications, new spectrum at millimeter-wave (mmWave) frequencies is being explored and been made available [2]. For the design and standardization of transceivers, we need to understand the channel characteristics in the mmWave frequency bands where they will operate. For example, environments such as offices can create numerous reflections, or multipath components (MPCs), that arrive at the receiver as delayed copies of the transmitted signal.

Receivers are typically designed with error correction and/or equalization designed to handle this distortion. Thus, understanding the dominant propagation mechanisms in these new radio bands has recently become of great interest to the research community [3–12]. Characterization of wireless environments is often accomplished by measuring the channel characteristics with a channel sounder. However, channel sounders utilize real, nonideal, electronic components, which often become even less ideal at mmWave frequencies. Additional measurements errors common to channel sounders include position inaccuracy, user error, signal distortions, and distortion due to imperfect antenna characteristics and interference. Thus, methods to quantify impairments in the received signal due to the performance of the hardware separately from impairments due to the channel are of increasing importance.

As an example, Fig. 1(a) shows the power delay profile (PDP) derived from a channel-sounder measurement. The PDP illustrates that components of the received signal are delayed and attenuated due to reflections. Ideally, once these primary channel impairments have been identified, a model of the channel can be created to use for standards activities, system design, and to create channel emulators that can replicate and test devices under conditions that are similar to those in which they will be deployed.

An example of such a model is given in Fig. 1(b), where the reflections illustrated in the PDP from Fig. 1(a) have been replicated as impulses whose magnitude and delay correspond a simplified version of the measured conditions. However, if the measured multipath components are due to hardware imperfections, such as internal reflections within the channel sounder, rather than channel characteristics, the model may be inaccurate.

Much of the prior work on channel-sounder performance verification was conducted “*in-situ*”; *i.e.*, in environments that are expected to provide specific propagation conditions during measurement campaigns or in uncontrolled laboratory environments [13–21]. For example, an in-situ verification is helpful prior to a measurement campaign by measuring the path loss of a relatively open environment with comparison to either a free-space or two-ray propagation models [22–23]. In addition to poor repeatability, when channel-sounder measurements made in these environments are compared to models such as map-based or ray-tracing models, assumptions about the reflective characteristics of the environment, positional accuracy [24] and the antenna characteristics of the sounder may increase uncertainty in the estimate of the

[1] Publication of the United States government, not subject to copyright in the U.S.

Submitted February 10, 2017.

J.N.H Dortmans was a Guest Researcher at NIST, Boulder, CO 80305 USA. He is now with the ASML (e-mail: jos.dortmans@asml.com).

Jelena Senic and Ruoyu Sun are Guest Researchers at NIST, Boulder, C) 80305 USA. (e-mail: Jelena.senic@nist.gov and ruoyu.sun@nist.gov)

J.T. Quimby, D.F. Williams, K.A. Remley and Peter B. Papazian are with the National Institute of Standards and Technology, Boulder, CO 80305 USA (e-mail: jeanne.quimby, dylan.williams, and kate.remley@ nist.gov and peter.papazian@nist.gov).

This article has been accepted for publication in a future issue of this journal, but has not been fully edited. Content may change prior to final publication. Citation information: DOI 10.1109/TAP.2019.2902623, IEEE Transactions on Antennas and Propagation

sounder's performance.

Other verification approaches use controlled conditions, involving channel-sounder measurements in, for example, anechoic chambers or conducted measurements of an artifact having "known" characteristics [13, 25–28]. A controlled condition can be implemented using two conducted cables with a combined and splitter [25]. The length of the cables may be chosen to simulate a ground bounce. The methods reported in the literature rely on the reported manufacturers' specifications in the controlled environments that were utilized.

The method presented here extends the controlled-condition concept, but requires no assumptions about the environment or the test object, because the artifact is characterized by a vector network analyzer (VNA) with a complete uncertainty analysis. The artifact design is limited to verification of sounders with removable antennas in static channels. For channel sounders with uncertainty analyses, overlapping error bars indicate agreement. However, even for sounders without complete uncertainty analyses, comparison to measurements of the artifact provides a degree of confidence in the measurements.

The artifact tests the ability of a channel sounder to resolve multipath components in delay and magnitude, providing a simplified channel for conducted measurements. Because it is designed with passive elements, it may be used over a wide frequency range (10 GHz to 62.5 GHz), providing a stable, repeatable, low-cost, portable system that is appropriate for round-robin testing across labs. With this artifact, we can simulate simple multipath environments by creating a direct path and up to two multipath components using different lengths of coaxial cable. We can create four different time delays in the multipath components and the attenuation of each multipath component can be controlled. To maximize repeatability between laboratories, the verification artifact is equipped with a temperature controller to ensure that the characteristics of the artifact do not change. While real propagation channels are typically more complex that the simple multipath configurations provided here, the goal of this work is to provide a stable, well-characterized environment for verification of mmWave channel-sounder hardware and channel metrics derived in post processing.

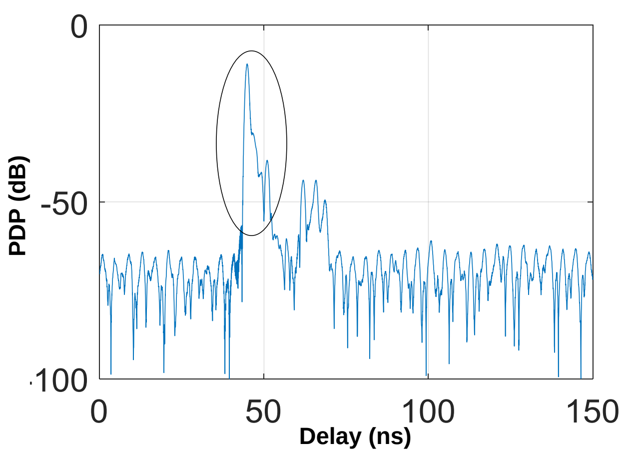

(a)

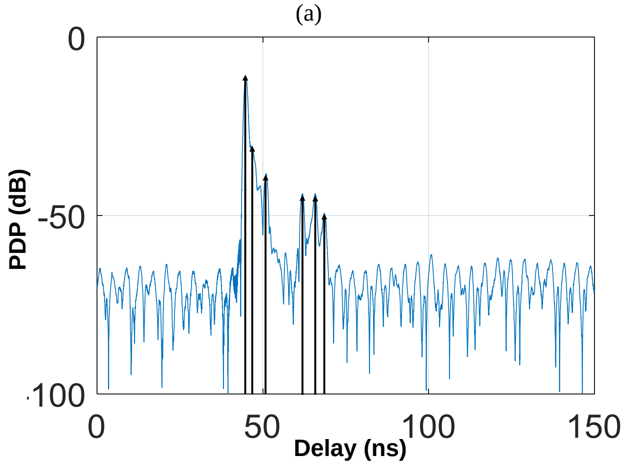

(b)

Fig. 1: (a) Power delay profile of a multipath environment measured by a channel sounder. (b) Simplified multipath environment for channel-sounder verification purposes.

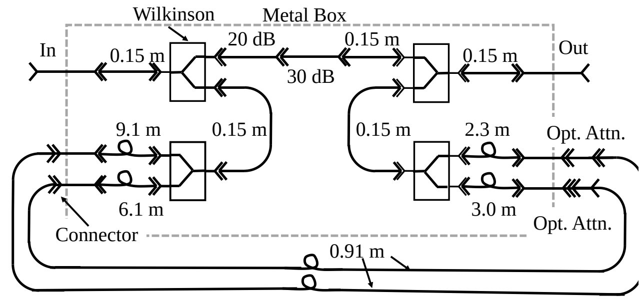

Fig. 2: Schematic of the verification artifact. All components inside the dashed rectangle are mounted inside a metal box.

In Section II, we describe the design and specifications of the verification artifact. Section III gives the theoretical background for the analysis performed in this paper. In Section IV, we characterize the verification artifact over a broad frequency band, with measurements uncertainties and as a function of temperature. An illustrative example in which we verify the performance of a 60.5 GHz channel sounder is described in Section V. We summarize the paper in Section VI.

II. Verification Artifact Design

A. *Creating a Repeatable Multipath Environment*

Figure 2 shows a schematic of the verification artifact. All components inside the dashed rectangle are mounted inside a metal box. To simulate a multipath environment, we used power dividers to split the signal into paths providing different delays. We used coaxial components with 1.85-mm connectors having a cut-off frequency of 67 GHz. Inside the verification artifact, we used cables of different lengths to create the delays. These semi-rigid cables were wound around a metal spool to keep the verification artifact compact and for good thermal conduction.

One signal path travels through the box without adding extra delay, creating the direct path. The direct path is additionally attenuated by 50 dB to compensate for the attenuation in the long cables in the multipath sections and to protect the receiver

This article has been accepted for publication in a future issue of this journal, but has not been fully edited. Content may change prior to final publication. Citation information: DOI 10.1109/TAP.2019.2902623, IEEE Transactions on Antennas and Propagation

hardware from overload.

After splitting the signal into a direct path and a multipath, the multipath signal is split again to create two multipath components. One part is fed to a 6.096 m (20') long cable and the other path is fed to a 9.144 m (30') long cable. These cables can be connected externally to create additional signal delays. With these cables, delays similar to those in indoor environments such as [17] can be created.

Attenuation can be added to the multipath sections to create different simulated environments. The locations of these optional attenuators are shown in Fig. 2. The attenuation that we apply to the multipath components depends on the desired frequency band because of the frequency dependent loss in the cables and the dynamic range of the channel sounder.

The connection options (with an example shown in Fig. 3), that realize different delays, are summarized in Table I. Internal cables 6.096 m and 9.144 m may be connected externally to 2.286 m or 3.048 m cables through different values of attenuation. Using these different configurations, the channel sounder verification box may create a direct path ("*D*") with a single peak in the PDP, single multipath ("*SM*") with two peaks in the PDP and double multipath ("*DM*") with three peaks in the PDP. The last column gives the delay times of the multipath components (MPCs) relative to the direct path.

B. Temperature Control

We want the multipath environment created by the artifact to be stable and repeatable and to be able to characterize channel sounders with good repeatability from lab to lab. To achieve this, we apply temperature control to the verification artifact because most components in the artifact (*e.g*., cables, dividers, and attenuators) are temperature sensitive. To distribute the heat inside the box, all components are mounted on a metal plate and the box is insulated. We maintain the temperature using Peltier elements controlled by a commercially available proportional–integral–derivative (PID) temperature controller. The Peltier elements are placed on the back of the metal plate to which we have mounted a heat sink with a fan. With this arrangement, we achieve temperature stability of ±0.05° C at the sensor of the temperature controller, which is the rated limit of the controller. Based on measurements, the warm-up time of the verification artifact is approximately 45 minutes.

TABLE I
MULTIPATH SET-UPS THAT CAN BE SIMULATED WITH THE VERIFICATION ARTIFACT

Set-up Config.	Name	Internal 6.096 m cable connected to	Internal 9.144 m cable connected to	MPC Delay(s) relative to Direct (ns)
Direct	*D*	2.286 m w/atten	3.048 m w/atten	--
Single Multipath	*SM1*	2.286 m no atten	3.048 m w/atten	53.8
	SM2	3.048 m no atten	2.286 m w/atten	57.3
	SM3	3.048 m w/atten	2.286 m no atten	68.3
	SM4	2.286 m w/atten	3.048 m no atten	71.9
Double Multipath	*DM1*	3.048 m no atten	2.286 m no atten	57.3 and 68.3
	DM2	2.286 m no atten	3.048 m no atten	53.8 and 71.8

Fig. 3 shows a photograph of the verification artifact connected to a National Institute of Standards and Technology (NIST) 60.5 GHz channel sounder described in [21]. The heat sink for temperature control is visible on top of the verification artifact. The cables on the sides of the verification artifact are the input and output cables connected to one of eight transmit ports, at left, and one of 16 receive ports, at right. We used 1.85 mm coax-to-waveguide adaptors to connect to the channel-sounder waveguide ports. Other adaptor types can be used to connect to other types of channel sounders. In Fig. 3, waveguide ports are connected to the remaining channels. The cables in the front of the verification artifact control the multipath components, as discussed above.

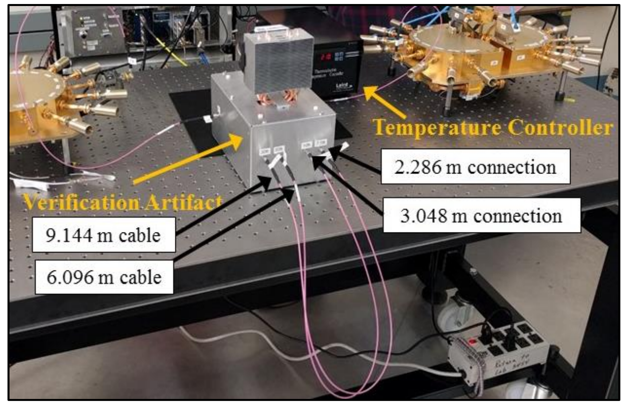

Fig. 3: A picture of the verification artifact connected to a 60.5 GHz channel sounder. The heat sink is visible in top of the verification artifact. The flexible cables in front of the verification artifact control the multipath components. The input and output cables are positioned on the sides of the verification artifact.

III. CHANNEL PARAMETERS AND METRICS

We will define key parameters and metrics to be used in the analysis of our channel-sounder verification artifact.

A. Power Delay Profile

A wireless radio channel can be characterized by the complex impulse response $h(\tau)$. The *power delay profile* is the magnitude squared of the impulse response of the channel, often given as

$$PDP(\tau) = |h(\tau)|^2, \quad (1)$$

where τ refers to the delay relative to the start of the transmitted signal. The PDP provides the path loss as a function of the time delay. Integrating the PDP over τ can provide the path loss (often represented as a negative value of "path gain") for a given fixed channel.

For static channels, the PDP can also be calculated from S-parameters measured with a VNA. To obtain the channel impulse response from VNA measurements, we transform the

This article has been accepted for publication in a future issue of this journal, but has not been fully edited. Content may change prior to final publication. Citation information: DOI 10.1109/TAP.2019.2902623, IEEE Transactions on Antennas and Propagation

measured forward transmission coefficient to the time domain by use of the inverse Fourier transform:

$$h(\tau) = IFFT(S_{21}), \tag{2}$$

where the Fast Fourier Transform may be used because the VNA measures at discrete frequencies. The time step of the resulting PDP depends on the bandwidth of the VNA measurements:

$$\Delta\tau = \frac{1}{BW} , \tag{3}$$

where $\Delta\tau$ is the time step and BW is the bandwidth of the measured S parameter data.

The maximum delay $\tau_{\max}$ that can be observed from a given sounder or VNA measurement depends on the bandwidth and frequency spacing as

$$\tau_{\max} = \Delta\tau N = \frac{N}{BW} = \frac{1}{\Delta f} , \tag{4}$$

where N is the number of frequency points in the measured bandwidth and Δf is the frequency step used for the VNA measurements. N should be chosen such that $\tau_{\max}$ is larger than the longest expected delay in the multipath environment.

B. *Wireless Channel Metrics*

Various wireless channel metrics can be calculated from the PDP. In this paper, we calculate the *RMS delay spread* (τ_{RMS}) *delay window*, *delay interval*, and the *number of multipath components*. These metrics come from the International Telecommunication Union – Recommendation (ITU-R) P.1407-5 [30], but other metrics may be derived with this approach. Fig. 4 shows an example of a PDP with a pictorial representation of these metrics and thresholds.

The value of τ_{RMS} for a given environment may be calculated from the square root of the second central moment of the PDP [30,31]:

$$\tau_{\mathrm{RMS}} = \sqrt{\frac{\int_0^\infty (\tau-\tau_0)^2 PDP(\tau) d\tau}{\int_0^\infty PDP(\tau) d\tau}} , \tag{5}$$

where τ_0 is the *mean delay* of the channel given by

$$\tau_0 = \frac{\int_0^\infty \tau PDP(\tau) d\tau}{\int_0^\infty PDP(\tau) d\tau} . \tag{6}$$

Typically, only values of the PDP above a certain threshold are used for the calculation of τ_{RMS}. This *multipath threshold* is often set with respect to the highest peak in the PDP, as shown in Fig. 4. Standards may specify the multipath threshold. If the receiver is very sensitive, a threshold far below the highest peak may be used to calculate τ_{RMS} and other metrics. In practice, most wireless device receivers have limited sensitivity, so the threshold is often quite high. For example, [30] recommends a threshold of −20 dB.

The *delay window* is defined as the portion of the PDP containing a certain percentage of the power above a defined noise floor. We use a common value of 90% for the power level in the delay window.

The *delay interval* corresponds to the interval between the time that the PDP first exceeds a certain threshold and the time

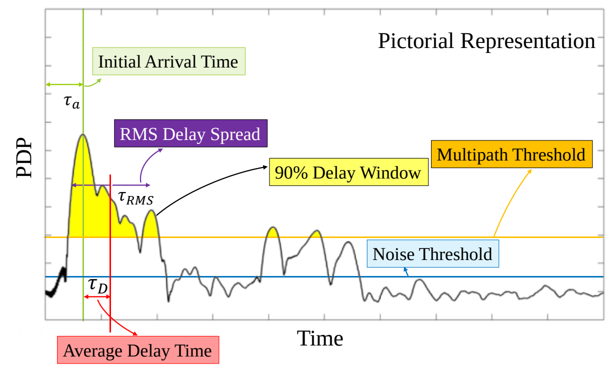

Fig. 4: Example of a PDP with indicated metrics and thresholds [30]).

when it falls below that threshold for the last time. In the present work, we use a threshold just above the noise floor of the PDP.

The *number of multipath components* (Number MPCs) is the number of peaks that exceed the multipath threshold. The multipath peaks also must exceed the noise threshold.

IV. Characterization of the Verification Artifact

A. *VNA Measurements and Uncertainty*

We characterized the artifact with a VNA to provide a comprehensive uncertainty analysis. This enables use of the verification artifact as a transfer standard.

1) *Calibration and Uncertainty Analysis*

We calibrated our VNA measurements of the artifact with a SOLT calibration and performed a comprehensive uncertainty analysis including systematic and random errors in post processing with the NIST Microwave Uncertainty Framework [31]. The Framework includes a drag-and-drop toolkit for managing the propagation of error in time and frequency domains. For systematic errors in the VNA measurements, models of the calibration standards are created, and uncertainties are found by iteratively varying the model parameters. This leads to both a linear error-propagation sensitivity analysis and a non-linear error propagation Monte-Carlo analysis. [25] Other systematic errors include impedance mismatch, loss in the cables and connectors and frequency response of the source and receiver, and directivity and cross talk due to signal leakage. Random errors were captured through multiple measurements and quantified using the error-propagation statistical analyses [31, 32].

The Framework accounts for the correlations between uncertainties at different frequencies so that uncertainties can be propagated through complex transforms such as the Inverse Fourier Transform that is used to calculate a PDP. Random errors from repeat measurements can be captured as well; see [31] and an application of the framework in [32].

This article has been accepted for publication in a future issue of this journal, but has not been fully edited. Content may change prior to final publication. Citation information: DOI 10.1109/TAP.2019.2902623, IEEE Transactions on Antennas and Propagation

2) *Wideband Measurements: 10 GHz to 50 GHz*

We measured the verification artifact over a wide band of frequencies to investigate its overall performance. S-parameters were measured from 10 GHz to 50 GHz with a frequency spacing of 5 MHz, resulting in 8001 measured frequency points. We set the VNA output power to –17 dBm and the IF bandwidth to 50 Hz. The temperature of the verification artifact was set to 21 °C. We measured every set-up ten times to reduce the noise and assess repeatability. We applied a sinc-squared filter with 40 GHz bandwidth to the S-parameter data for the calculation of the PDPs. This filter reduces the side lobes when converting from S-parameters in the frequency domain to the PDP in the time domain.

Fig. 5(a) shows the results of the Direct path (*D)* set-up described in Table I. For the Double-Multipath (*DM1*) set-up shown in Fig. 5(b), we added 20 dB of attenuation to the first multipath component and 16 dB to the second multipath component in order to obtain a low attenuation in the direct path relative to the attenuation in the multipath components, which is common in real environments.

The graphs in Fig. 5 show the PDP, the standard uncertainty and 95 % confidence interval for the VNA measurements transformed to the time domain.

Fig. 5(b) shows a significant amount of close-in multipath, having delays close in time to that of the direct path delay, as well as reflections at around 10 ns, 57 ns and 68 ns. Impedance mismatches in the portable artifact due to the coaxial cables and connectors cause these many close-in reflections.

In Fig. 5(b), the first and second multipath components lay approximately 2.22 dB and 4.05 dB below the direct-path peak, respectively. The standard uncertainty (Std. Unc.) of these measurements is ± 1.10 dB. Thus, the −20 dB multipath threshold of [30] would allow resolution of both multipath components. Lower thresholds may be used as well, which could enable characterization of channel sounders with high dynamic ranges.

To illustrate this, Table II shows values of various metrics calculated from the measured *DM1* PDP for different multipath threshold values. The delay window (59.00 ns) and delay interval (59.13 ns) are not dependent on the multipath threshold, so these values are constant for this table.

For thresholds of −5 dB and lower, all three peaks are included in the calculation of τ_{RMS}, resulting in a similar value of τ_{RMS} for all lower thresholds. For a multipath threshold of −10 dB and lower, an unintentional multipath component is detected, increasing the number of multipath components to four. This component of low magnitude; therefore, τ_{RMS} does not change significantly.

The results for the other set-ups calculated over the wideband 10 GHz – 50 GHz frequency range are given in Table III for a multipath threshold of −20 dB and a noise threshold of −95 dB.

TABLE II
WIDEBAND WIRELESS CHANNEL METRICS FOR SET-UP *DM1*.

Multipath Threshold (dB)	τ_{RMS} (ns)	Number MPCs
−1	0.01	1
−3	22.27	2
−5	26.01	3
−10	26.36	3
−20	26.28	3
−30	26.28	4
−40	26.28	4
−50	26.28	4

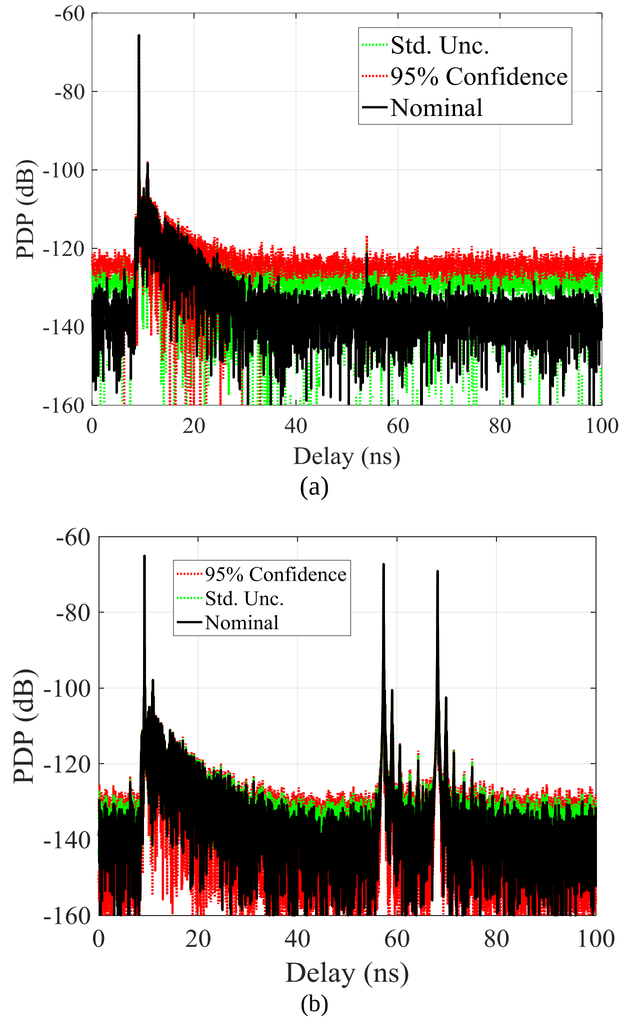

Fig. 5: PDP of (a) the Direct path set-up and (b) the Double-Multipath 1 set-up calculated from VNA measurements (black) between 10 GHz and 50 GHz. The green lines indicate the standard uncertainty. The red lines indicate the 95 % confidence interval.

TABLE III
WIDEBAND WIRELESS CHANNEL METRICS FOR ALL POSSIBLE SET-UPS.

Name	τ_{RMS} (ns)	Delay Window (ns)	Delay Interval (ns)	Number MPCs	MPCs Power (dB)
D	0.01	0.04	0.12	1	-65.04
SM1	22.01	44.62	44.79	2	-64.76
SM2	23.91	48.15	48.26	2	-67.23
SM3	28.21	59.01	59.13	2	-69.13
SM4	26.92	62.53	62.64	2	-71.46
DM1	26.29	59.00	59.13	3	-67.26, -69.09
DM2	23.85	62.51	62.64	3	-64.77, -71.48

This article has been accepted for publication in a future issue of this journal, but has not been fully edited. Content may change prior to final publication. Citation information: DOI 10.1109/TAP.2019.2902623, IEEE Transactions on Antennas and Propagation

Table III shows the range of multipath conditions that can be created with the verification artifact.

In the absence of multipath, the value of τ_{RMS} for the Direct *D* channel in Table III and the delay window should be theoretically zero due to an infinite bandwidth. However, the VNA measurements cover a finite bandwidth, leading to a nonzero value for these parameters. If the channel contains dispersion and reflections at the ports, the VNA will capture this linear dispersion behavior and impedance mismatch. An example of such dispersion is shown in Section V. Note that, since these are small values of τ_{RMS}, a metric that captures the absolute differences in multipath magnitude and delay from a reference may be more appropriate than τ_{RMS} for our application.

3) *Temperature Measurements*

To investigate the effect of temperature on the verification artifact's characteristics, we performed VNA measurements for various settings of the PID controller over a temperature range between 10 °C and 30 °C. We again measured the *DM1* set-up from Table I. In this case, we added 6 dB of attenuation to the shortest multipath component to prevent it from being stronger than the direct path.

We measured 4001 points between 30 GHz and 50 GHz with an IF bandwidth of 50 Hz and VNA transmit power of −17 dBm. The frequency band was reduced to save measurement time. We took five measurements per temperature to reduce noise. A sinc-squared filter with bandwidth of 40 GHz was again applied to the S-parameter data for the calculation of the PDPs.

Fig. 6(a) illustrates the influence of temperature on the PDP. We zoomed in on the second multipath peak because this path has the longest cable configuration and so is most influenced by temperature. The second multipath peak in the PDP is clearly attenuated with temperature, from to -85.4 dB to -90.18 dB for temperatures ranging from 10 °C to 30 °C. As temperature increases, the metal resistance in the cables also increases. This is easily seen from a simulation of the effects of temperature on resistance with 20 ºC as a reference temperature shown in Fig. 6(b). From this simulation, it may be readily seen that increasing the temperature also increases the resistance of metal. This increase in resistance may explain the increase in attenuation, although further investigation is warranted.

There is also a small decrease in the delay with increasing temperature. This effect is caused by the temperature dependence of the dielectric material in the coaxial cables [33], resulting in a higher wave propagation velocity for the cables. The time difference between the 10 °C peak and the 30 °C peak is about 0.04 ns, which translates to a change in relative permittivity of about 0.003. This is of the same order of magnitude (0.007) that Ref. [33] reports for a temperature change of 20 °C.

To investigate the effect of the temperature on calculated PDP metrics, we calculated τ_{RMS} for all temperature measurements and used different multipath thresholds for the calculations. The results are shown in Fig. 6(c), where we drew a linear fit through the data points. The value of τ_{RMS} decreases with increasing temperature due to the increasing attenuation of the coaxial cables. This figure gives insight into the effect of the multipath threshold. For a threshold of −10 dB, only the direct

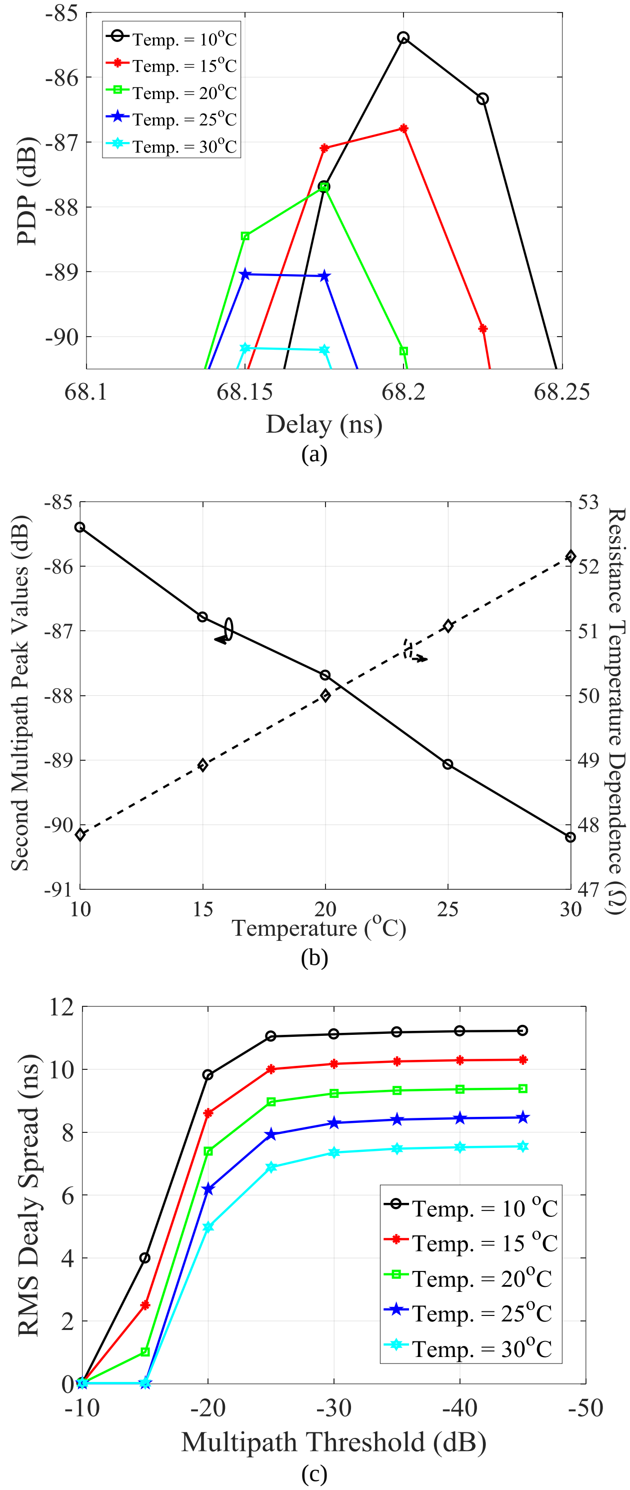

Fig. 6: (a) PDPs of the *DM1* set-up measured with different temperatures calculated for 30 GHz – 50 GHz. The plot is zoomed in on the second multipath peak to show the effect of the temperature, (b) Plot of measurement of the second multipath peak vs temperature and simulation of resistance temperature (c) Plot of τ_{RMS} of the *DM1* set-up as a function of multipath threshold for different verification artifact temperatures.

path is detected in the calculation of τ_{RMS} so the spread is very low, essentially zero, as shown at the lower left corner of Fig.

This article has been accepted for publication in a future issue of this journal, but has not been fully edited. Content may change prior to final publication. Citation information: DOI 10.1109/TAP.2019.2902623, IEEE Transactions on Antennas and Propagation

6(c). For a threshold of −15 dB, only a single multipath peak with an RMS delay spread of 4 ns is detected for a temperature of 10 °C and lower values of RMS delay spread for higher temperatures. Thresholds of −25 dB and lower take all the multipath peaks into account. Lowering the threshold below −25 dB does not change the τ_{RMS} significantly for a given temperature.

The temperature of the verification artifact has a stability of ±0.05 °C. Consequently, there is an uncertainty of 0.01 ns for τ_{RMS} as a function of temperature. Future work will incorporate this into our analysis. Also, more research should be conducted on the frequency dependence of this uncertainty. We now only have experimental results for a frequency range of 30 GHz to 50 GHz.

4) Reproducibility

To test reproducibility, measurements of the same set-up were made on different days. The cables were also moved, disconnected and reconnected between the measurements. This resulted in a significant difference in measured magnitude and phase. Fig. 7(a) shows $|S_{21}|$ of the *DM1* setup measured on three different days. Because this is not a correctable error, the difference in $|S_{21}|$ between the various days was added as an systematic component uncertainty in the Microwave Uncertainty Framework analysis.

In Fig. 7(b), we plot the phase difference between the first measurement and the measurements on the other days. Averaging the S-parameters in the frequency domain first requires phase alignment. A simple method of averaging the results is to first convert the data to the time domain by calculating the PDPs for each day and averaging the resulting PDPs.

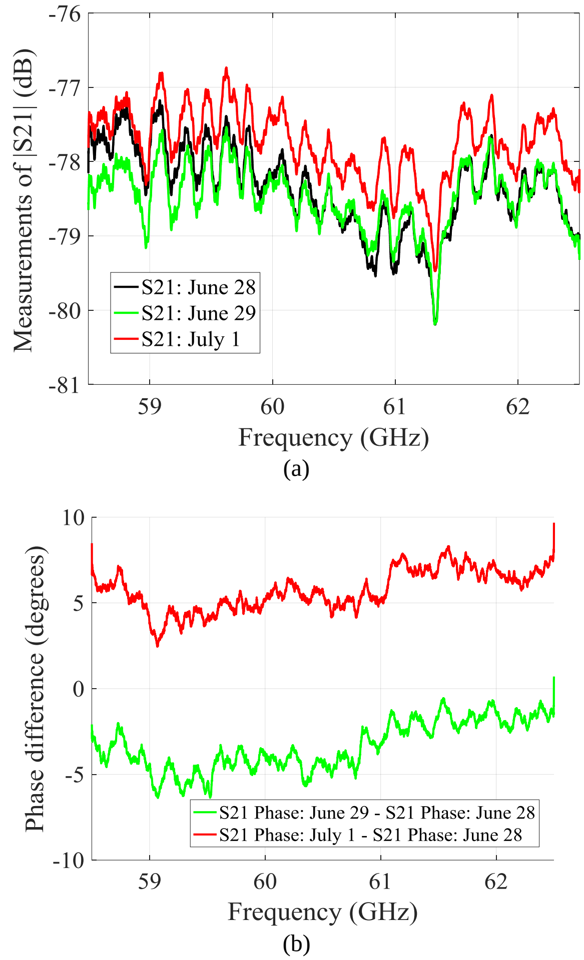

Fig. 7: (a) $|S_{21}|$ of the Double-Multipath 1 (*DM1*) set-up measured on six different days. (b) Phase difference of the *DM1* set-up between the first measurement and measurements on different days. In both (a) and (b), the data were smoothed with a 55-point averaging window for better visualization.

V. Channel-Sounder Verification

A. VNA Measurements

We next demonstrate the verification process on a 60.5 GHz channel sounder. As discussed earlier, to verify the performance of a channel sounder, we first perform a VNA measurement of the artifact over the frequency range where the channel sounder operates. The channel sounder in this example operates between 58.5 GHz and 62.5 GHz (null-to-null bandwidth). To compare metrics such as delay window and number of multipath components, we must produce a PDP with the same length as the channel sounder's PDP, which is, in this case, 1023.5 ns. The minimum number of points needed with VNA measurements to obtain a PDP of the same length as the channel sounder can be calculated from (4), which results in $\tau_{\max} \times BW = 4094$ points. We doubled the number of frequency points to reduce the measurement noise and added one point to get a frequency spacing that can be represented with a fixed number of digits. So, we measured 8189 frequency points from 58.5 GHz to 62.5 GHz. In post processing, we applied the same filter as the channel sounder uses in the pseudorandom noise code (see below) to the S-parameter data for the calculation of the PDPs.

We also included the 1.85-mm-to-WR-15 waveguide adapters in our VNA measurements to match the channel sounder's connector type. Thus, the VNA calibrations were performed with a WR-15 calibration kit. We also included an isolator at the transmitter side because this was included in the channel-sounder measurements. To further reduce the measurement noise, we conducted multiple measurements for each artifact set-up. We repeated these groups of measurements six times. For each group of measurements, we disconnected and reconnected all of the cables to investigate the effect of cable movement. For the first three groups of measurements, 10 repeat measurements were averaged and for the last three groups of measurements, three repeat measurements were averaged. From these data, PDPs were calculated, metrics computed, and uncertainties estimated.

B. Channel-Sounder Measurements

Having measured the verification artifact with the VNA, we next measured the artifact with the 60.5 GHz channel sounder. Differences between the measurements will give information about the hardware performance of the channel sounder.

The channel sounder transmits a pseudorandom noise (PN) code occupying a null-to-null bandwidth of 4 GHz. For the configuration tested, the period of one codeword was 1023.5 ns

This article has been accepted for publication in a future issue of this journal, but has not been fully edited. Content may change prior to final publication. Citation information: DOI 10.1109/TAP.2019.2902623, IEEE Transactions on Antennas and Propagation

and was generated by an arbitrary waveform generator producing a BPSK modulated 3 GHz IF signal. This signal was upconverted to 60.5 GHz, bandpass filtered, and amplified before being transmitted. The transmitter has an array of eight WR-15 scalar-feed horn antennas oriented at azimuthally spaced angles of 22.5° to generate a variety of angles-of-departure. The power amplifiers associated with each antenna are electronically controlled to select individual transmit horn antennas.

A similar form of antenna switching is used on the receive side in order to obtain angle-of-arrival information. One of 16 horn antennas is selected by electronically controlling 16 low-noise amplifiers with a switching speed of approximately 35 ns. The received signal is downconverted and digitized at 3 GHz. Correlation with the transmitted PN code is done in the post-processing to provide the complex impulse response of the channel. The length of the PN codeword determines the correlation gain. The receive array can be placed on robotic positioning systems that are suitable for indoor and outdoor use. A typical measurement sweeps through all eight transmit antennas and 16 receive antennas. The time to sample all eight transmit and 16 receive antennas is approximately 262 μs. Pre-distortion filters generated from back-back tests were employed to remove non-ideal effects from TX and RX electronic devices [21]. A more detailed description of the NIST correlation-based channel sounder, shown in Fig. 3, can be found in [21].

PN sequences were measured between one transmit channel and one receive channel after antenna removal, as shown in the configuration of Fig. 3. Fig. 8 shows a PDP of the Direct and Double-Multipath 1 set-up measured with the VNA including measurement uncertainty. We also plot the PDP obtained from a single channel-sounder measurement. The PDPs are normalized, with the direct path set to 0 dB and its arrival time to the VNA arrival time. Note that the level of the multipath components is much lower compared to the wideband measurements in Fig. 5, due to cable loss.

In Fig. 8, we have circled the biggest differences between the VNA and channel-sounder PDPs. Before the direct-path peak, the channel sounder measures a peak above the noise floor. Also, at 28 ns, the channel sounder measures a peak that is not visible in the VNA measurements. These peaks occur approximately 40 dB below the highest peak so their effect on most wireless metrics will be minimal.

The peak that arrives before the direct path peak may be caused by over-the-air leakage of the signal through the waveguide-to-coax adapters. We encountered problems with leakage in the VNA measurements and added conductive epoxy to the adapters, which removed the leakage. The adapters in the channel-sounder measurements were positioned closer together and had a different orientation than with the VNA measurements. Possibly, there is still some leakage with this position and orientation.

In Fig. 9, we have zoomed in on the main peak. Internal reflections due to impedance mismatches and imprecise calibrations could create additional reflections or ripples near the main peak and other multipath peaks. The channel sounder would not be able to resolve the ripples from the main peak since they are too closely spaced in time. The channel sounder would then have the effect of broadening the main peak. This effect quantitatively can be seen in Table IV, where for a multipath of threshold -20 dB corresponding to a single line-of-sight signal only, τ_{RMS} channel sounder (CS) is 0.03 ns larger than τ_{RMS}VNA. Such broadening occurs around each multipath component as well.

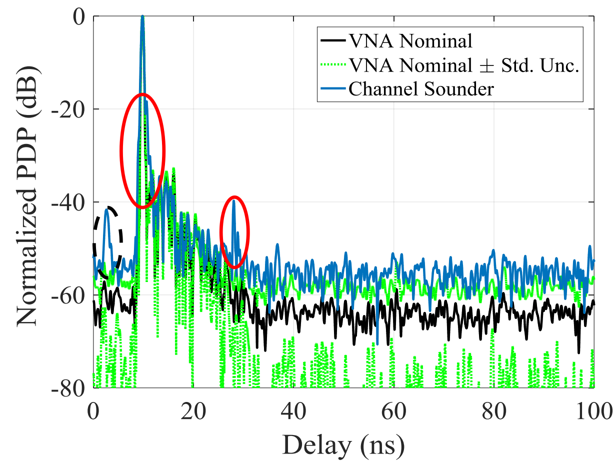

(a)

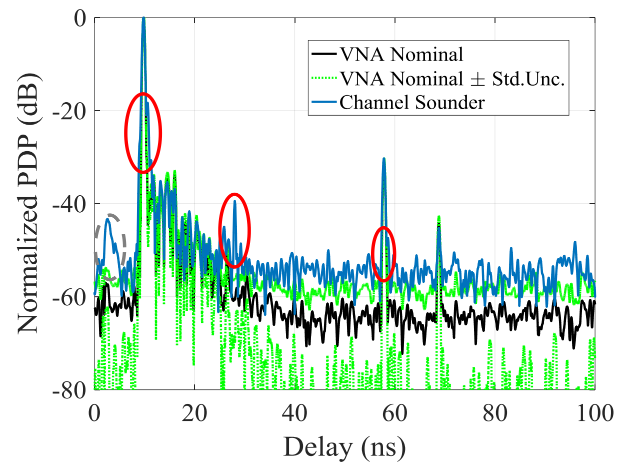

(b)

Fig. 8: PDP of VNA (black) and channel-sounder (blue) measurements of the (a) Direct (*D*) and (b) Double-Multipath 1 (*DM1*) set-ups. The circles show the most significant differences between the VNA and channel-sounder PDPs. The channel-sounder did not have an amplitude scaling or consistent time start when the measurements were made.

Table IV shows various wireless channel metrics calculated from the PDPs of Fig. 8(b) for different multipath threshold values. The noise thresholds were set to −145 dB resulting in a similar noise floor as the channel sounder. The number of multipath components for the VNA can be a fraction because the wireless channel metrics are composed of an average of multiple repeat measurements.

Note that the value of τ_{RMS} is much smaller than that of the wideband measurement because of the significant loss in the cables that represent the multipath components. Nonetheless,

This article has been accepted for publication in a future issue of this journal, but has not been fully edited. Content may change prior to final publication. Citation information: DOI 10.1109/TAP.2019.2902623, IEEE Transactions on Antennas and Propagation

τ_{RMS} and the number of multipath components remain

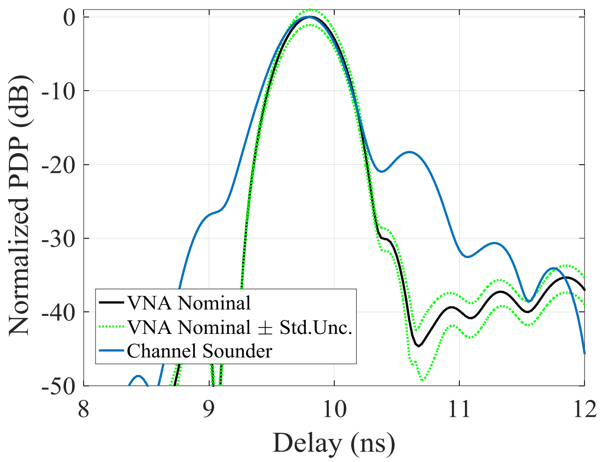

Fig. 9: Zooming-in on the PDP in Fig. 8(b) shows an effective broadening of the main peak due to internal reflections within the channel sounder.

dependent on the multipath threshold.

Comparing columns two and three of Table IV, we see that τ_{RMS} as measured by the channel sounder, is generally higher than the VNA measurements and, for threshold values below −35 dB, exceeds the standard uncertainty of the VNA measurements. This can be explained by the effective broadening of the multipath peaks measured by the channel sounder as shown in Fig. 9, which results in a higher τ_{RMS}. The as-yet unknown uncertainty of the channel sounder measurements will determine whether or not this difference is significant (that is, if the error bars overlap, the difference would not be considered significant).

The Delay Windows are 0.52 ± 0.00 ns for the VNA and 0.59 ns for the channel sounder. The difference in the Delay Window can again be explained by the effective pulse broadening due to internal reflections in the channel sounder. The Delay Intervals are 60.28 ±0.08 ns for the VNA and 66.80 ns for the channel sounder. The Delay Interval of the channel sounder is higher because of the peak that appears in front of the direct path peak in the channel-sounder measurement which, as noted, may be a measurement artifact. Finally, note that the channel sounder measures an extra multipath component at a multipath threshold of −20 dB. This extra multipath component is visible in Fig. 9 at about 10.6 ns and is likely due to an internal reflection. While these differences are not likely to significantly change the common wireless metrics presented here for a multipath threshold of, for example, −20 dB, they do indicate nonidealities in the channel sounder which might need to be addressed, depending on the application. Note: The number of channel sounder's MPCs goes up and down around the threshold values of -20 and -30 dB. This is due to a rounding error.

TABLE IV: WIRELESS CHANNEL METRICS FOR DIFFERENT MULTIPATH THRESHOLDS CALCULATED FROM VNA AND CHANNEL-SOUNDER (CS) MEASUREMENTS AT 60.5 GHZ.

Multipath Threshold (dB)	τ_{RMS} VNA (ns)	τ_{RMS} CS (ns)	Number MPCs VNA	Number MPCs CS
−10	0.15 ±0.00	0.15	1.00 ±0.00	1
−20	0.15 ±0.00	0.18	1.00 ±0.00	2
−30	0.16 ±0.00	0.19	1.00 ±0.00	1
−35	1.29 ±0.03	1.37	4.00 ±0.11	3
−40	1.38 ±0.03	1.46	8.00 ±2.45	7
−45	1.43 ±0.03	1.49	14.00 ±1.73	11

VI. CONCLUSION

We designed a portable artifact for verification of channel sounders at millimeter-wave frequencies. This artifact is characterized with a VNA and measured with a channel sounder to verify the performance of the latter. We characterized the artifact for frequencies between 10 GHz and 62.5 GHz. The artifact is able to simulate different multipath environments with a direct path and up to two delayed multipath components. A variety of channel metrics can be created, but importantly, the uncertainties in these metrics can be derived from the VNA measurements.

The verification artifact is equipped with temperature control in order to ensure a stable environment. This is important because of the temperature dependency of the attenuation in the long cables and its effect on characteristics such as τ_{RMS} where we found, for example, that for a multipath threshold of -25 dB τ_{RMS} ranges from 9.81 ns to 4.98 ns for a temperature range of 10 to 30 ºC, respectively.

Reproducibility tests of the artifact show that a significant component of uncertainty in the VNA measurements is due to the variation in $|S_{21}|$ over time. A possible source of the uncertainty may be the flexible cables that are used for the multipath sections and external connections to the artifact. These cables are not temperature controlled and are moved between measurements. Another source of uncertainty is the temperature stability within the artifact. The temperature stability is now measured by one sensor that is used by the temperature controller. Additional sensors could be used to determine if the temperature is stable throughout the box. We also demonstrated that phase alignment is needed to average the measurements due to drift over time. To simplify averaging, we averaged in the time domain by averaging PDPs.

We used the verification artifact to assess the performance of a 60.5 GHz channel sounder. The results showed that the channel sounder measures broader peaks than the VNA possibility due to unresolvable internal reflections, which could lead to errors in the estimate of RMS delay spread and the number of multipath components for certain threshold values. We also detected artificial multipath peaks in the channel-sounder measurements that were not present in the VNA measurements. These may, in some circumstances, affect the value of the RMS delay spread.

The artifact is intended for the verification of channel sounders at millimeter-wave frequencies. We may, upon request, make available the portable artifact for individual laboratories, universities, companies or round-robin campaigns

This article has been accepted for publication in a future issue of this journal, but has not been fully edited. Content may change prior to final publication. Citation information: DOI 10.1109/TAP.2019.2902623, IEEE Transactions on Antennas and Propagation

across laboratories. The high dynamic range of the VNA and the traceable uncertainty analysis provide a rigorous method for evaluating a wide variety of channel sounders. Currently, there are few alternatives that characterize the hardware effects of channel sounders in these bands other than comparison to free-space theory.

ACKNOWLEDGEMENT

The mmWave channel sounder used in this paper resulted from the extensive modeling and processing support from NIST colleagues Camillo Gentile, Nada Golmie, and from Institute for Telecommunication Sciences (ITS) colleague Yeh Lo who helped to develop and test the sounder.

REFERENCES

[1] Cisco. *Cisco Visual Networking Index: Global Mobile Data Traffic Forecast* [Online]. Available: https://www.cisco.com/c/en/us/solutions/collateral/service.../vni-forecast-qa.pdf

[2] Federal Communications Commission, "Use of Spectrum Bands Above 24 GHz for Mobile Radio Services, FCC-16-89," July 2016, [Online] Available: https://apps.fcc.gov/edocs_public/attachmatch/FCC-16-148A1.pdf.

[3] D. Beauvarlet and K. Virga, "Measured characteristics of 30-GHz indoor propagation channels with low-profile directional antennas," *IEEE Antennas and Wireless Propagation Letters*, vol. 1, no.1, pp. 87-90, 2002.

[4] N. Moraitis and P. Constantinou, "Indoor channel measurements and characterization at 60 GHz for wireless local area network applications," *IEEE Trans. Antennas and Propagat.*, vol. 52, no. 12, pp. 3180 -3189, Dec. 2004.

[5] S. Geng, J. Kivinen, X. Zhao, and P. Vainikainen, "Millimeter-wave propagation channel characterization for short-range wireless communications," *IEEE Trans. Veh. Commun.*, vol. 58, no. 1, pp. 3–13, Jan. 2009.

[6] M. Peter and W. Keusgen, "Analysis and comparison of indoor wideband radio channels at 5 and 60 GHz," *3rd European Conf. on Antennas and Propagat. (EuCAP 2009)*, Berlin, Germany, Mar. 23-27, 2009, pp. 3830-3834.

[7] M. Kyro, K. Haneda, J. Simola, K. Nakai, K.-i. Takizawa, H. Hagiwara, and P. Vainikainen, "Measurement based path loss and delay spread modeling in hospital environments at 60 GHz," *IEEE Trans. Wireless Commun.*, vol. 10, no. 8, pp. 2423–2427, Aug. 2011.

[8] T. S. Rappaport, S. Shu, R. Mayzus, H. Zhao, Y. Azar, K. Wang, G. N. Wong, J. K. Schulz, M. Samimi, and F. Gutierrez, "Millimeter wave mobile communications for 5G cellular: It will work!" *IEEE Access*, vol. 1, pp. 335-349, May 2013.

[9] J. Zhu, H. Wang, and W. Hong, "Large-scale fading characteristics of indoor channel at 45-GHz band," *IEEE Antennas and Wireless Propagation Letters*, vol. 14, pp. 735-738, Dec. 2014.

[10] G. R. MacCartney, T. S. Rappaport, S. Sun, and S. Deng, "Indoor office wideband millimeter-wave propagation measurements and channel models at 28 and 73 GHz for ultra-dense 5G wireless networks," *IEEE Access*, vol. 3, pp. 2388–2424, Oct. 2015.

[11] C. Gentile, J. Senic, P. B. Papazian, J.-K. Choi, and K. A. Remley, "Pathloss models for indoor hotspot deployment at 83.5 GHz," *IEEE Global Communications Conference: The First International Workshop on 5G Millimeter-Wave Channel Models* (*GLOBECOM 2016*), Washington D.C., USA, Dec. 2016, pp. 1-6.

[12] X. Wu, C.-X. Wang; J. Sun, J. Huang; R, Feng; Y. Yang; and X. Ge, "60 GHz millimeter-wave channel measurements and modeling for indoor office environments," *IEEE Trans. Antennas and Propagat.*, vol. 65, pp. 1912 – 1924, Feb. 2017.

[13] 5G mmWave Channel Model Alliance Wiki Website, https://sites.google.com/a/corneralliance.com/5g-mmwave-channel-model-alliance-wiki/home

[14] G. Matz, A. F. Molisch, F. Hlawatsch, M. Steinbauer and I. Gaspard, "On the systematic measurement errors of correlative mobile radio channel sounders," *IEEE Trans. Commun*., vol. 50, no. 5, pp. 808 – 821, May 2002.

[15] S. Kim, W. T. Khan, A. Zajić, and J. Papapolymerou, "D-band channel measurements and characterization for indoor applications," *IEEE Trans. Antennas and Propagat.*, vol. 63, no. 7, pp. 3198-3207, July 2015.

[16] Z. Wen, H. Kong, Q. Wang, S. Li, X. Zhao, M. Wang, and S. Sun, "mmWave channel sounder based on COTS instruments for 5G and indoor channel measurement," *2016 IEEE Wireless Commun. and Networking Conf. Workshops (WCNCW)*, April 3-6, 2016, p. 37 – 43.

[17] P. B. Papazian, J.-K. Choi, J. Senic, P. Jeavons, C. Gentile, N. Golmie, R. Sun, D. Novotny, and K.A. Remley, "Calibration of millimeter-wave channel sounders for super-resolution multipath component extraction," *10th European Conf. on Antennas and Propagat. (EuCAP 2016)*, Davos, Switzerland , Apr. 2016,pp. 1-5..

[18] P. B. Papazian, C. Gentile, K. A. Remley, J. Senic, and N. Golmie, "A radio channel sounder for mobile millimeter-wave communications: system implementation and measurement assessment," *IEEE Trans. Microw. Theory and Tech.*, vol. 64, no. 9, pp. 2924-2932, Sept. 2016.

[19] G. R. MacCartney and T. S. Rappaport, "A flexible millimeter-wave channel sounder with absolute timing," *IEEE J. Sel. Areas Comm*., vol. 35, no. 6, pp. 1402 – 1418, June 2017.

[20] J. Li, Y. Zhao, C. Tao, and B. Ai, "System design and calibration for wideband channel sounding with multiple frequency bands," *IEEE Access*, vol. 5, pp. 781–793, Jan. 2017.

[21] R. Sun, P. B. Papazian, J. Senic, Y. Lo, J. Choi, K. A. Remley, and C. Gentile, "Design and calibration of a double-directional 60 GHz channel sounder for multipath component tracking," *11th European Conf. on Antennas and Propagat. (EuCAP 2017)*, Paris, France, Mar. 19-24 2017, pp. 1-5.

[22] K. A. Remley, C. Gentile, A. Zajic and J. T. Quimby, "Methods for Channel Sounder Measurement Verification," *2017 IEEE 86th Vehicular Technology Conference (VTC-Fall)*, Toronto, ON, 2017, pp. 1-4.

[23] C. Cheng, S. Kim and A. Zajić, "Comparison of path loss models for indoor 30 GHz, 140 GHz, and 300 GHz channels," *2017 11th European Conference on Antennas and Propagation (EUCAP)*, Paris, 2017, pp. 716-720.

[24] J. Quimby, A. E. Curtin, D. R. Novotny, K. A. Remley, C. -. Wang and R. Candell, "Variability of sounder measurements in manufacturing facilities," *2016 IEEE International Symposium on Antennas and Propagation (APSURSI)*, Fajardo, 2016, pp. 1689-1690.

[25] J. Quimby, J. Jargon, R. Leonhardt, P. Hale, K. A. Remley, A. Koepke, S. Street, R. Johnk, C. Hammerschmidt, P. McKenna, I. Strange, N. DeMinco, J. Diener, J. Rezac, R. "Chad" Smith, C. Hoyt, and S. Springer, "Channel Sounder Measurement Verification: Conducted Tests" Technical Note (NIST TN) in progress

[26] M. Landmann, M. Käske, and R.S. Thomä, "Impact of incomplete and inaccurate data models on high resolution parameter estimation in multidimensional channel sounding," *IEEE Trans. Antennas and Propagat.*, vol. 60, no 2, pp. 557-573, Feb. 2012.

[27] Y. Chang, Y. Konishi, M. Kim, J.-i. Takada, "Calibration techniques for fully parallel 24 × 24 MIMO sounder," *Proc. 2012 Int. Symp. on Antennas and Propagat. (ISAP)*, Nagoya, Japan, Oct. 29 – Nov. 2 2012, pp. 331 – 334.

[28] S. Salous, S. Feeney, X. Raimundo, and A. Cheema, "Wideband MIMO channel sounder for radio measurements in the 60 GHz band," *IEEE Trans. Wireless Commun.*, vol. 15, no. 4, pp. 2825-2832, Apr. 2016.

[29] T.S. Rappaport, *Wireless Communications: Principles and Practice*, 2nd. ed., Prentice Hall, Upper Saddle River, NJ, 2015.

[30] ITU, International Union of Telecommunications. ITU-R P. 1407-5 Recommendation: Multipath propagation and parameterization of its characteristics., 2013. [Online]. Available at https:nnwww.itu.intn.

[31] D. F. Williams, NIST Microwave Uncertainty Framework, Beta Version NIST, Boulder, CO, USA, Jun. 2014, [Online]. Available: http://www.nist.gov/ctl/rf-technology/related-software.cfm

[32] D.F Williams, W. Zhao, R. A. Chamberlin, J. Cheron, and M. Urteaga, "Verification of a foundry-developed transistor model including measurement uncertainty," *87th ARFTG Microw. Meas. Conf. Dig.*, San Francisco, CA, USA, May 2016, pp. 1-4.

[33] P. Ehrlich, "Dielectric properties of teflon from room temperature to 314 C and from frequencies of 10^2 to 10^5 c/s," *Journal of Research of the National Bureau of Standards*, vol. 51, no. 4, Oct. 1953.